The Journal of Energy: Engineering & Management

Vol. 11, No. 4, Winter 2022, P. 60-73

Research Article

[DOR: 20.1001.1.23452951.1400.11.4.2.1]

[DOI: 10.22052.11.4.60]

Feasibility Study of Solar Ejector Cooling Cycle in Different Weather Conditions

Ali Khalilpour[1], MozaffarAli Mehrabian[2], Aghil Iranmanesh[3*]

[1] Department of Mechanical Engineering, Shahid Bahonar University of Kerman, Kerman, Iran
ali.khalilpoor@gmail.com

[2] Department of Mechanical Engineering, Shahid Bahonar University of Kerman, Kerman, Iran
ma_mehrabian@yahoo.com

[3] Department of Mechanical Engineering, University of Jiroft, Jiroft, Iran
iranmanesh.aghil@ujiroft.ac.ir

Received: 9/29/2020 **Accepted:** 7/30/2021

Abstract

Today, renewable energies are of more interest due to the depletion of the ozone layer, an increase in the cost of fossil fuels, and their friendliness with the environment. The sun is a great source of energy which is readily accessible. It has many applications in lighting, heating, and cooling. In this study the thermal performance of a solar ejector cooling cycle is evaluated using several different working fluids. The effect of operating conditions-- namely the generator, condenser, and evaporator temperatures-- on the system performance is also investigated. Based on weather conditions in different regions, the performance of ejector cooling cycle in several months of the year is also determined. The results show that the operating conditions have a determinant effect on cycle performance. It is observed that an increase in the generator exit temperature results in an increase in cycle coefficient of performance. It is also deduced that the rates of COP increase for the evaporator temperature ranges of 13-15°C and 7-9°C are about 8 and 6% respectively. It is also concluded that a larger collector area is required in warmer weather conditions.

Keywords: Ejector, Refrigeration, Solar collector, Solar energy.

* Corresponding autho

[DOR: 20.1001.1.23452951.1400.11.4.2.1]

[DOI: 10.22052.11.4.60]

1. Introduction

Due to the energy crisis in recent years and the demand for energy, especially in the summer, solar energy has attracted more attention. Compression refrigeration cycle has disadvantages such as high energy consumption and technical problems related to the compressor (manufacturing, lubrication, maintenance, and repairs). To eliminate these disadvantages, an ejector cooling cycle is proposed. In this cycle, the compressor is replaced by an ejector and a thermal solar collector.

Early studies were accomplished on ejector cooling system by Huang et al. [1]. They tried to increase the efficiency of these systems in a 1-D analysis. They also conducted their research on 11 different ejectors with R-141b as the working fluid to determine the effective parameters in the ejector optimum design. It was concluded that the rate of primary (flow from the generator) and secondary (flow from the evaporator) degrees of superheat were also two important factors in the refrigeration system performance. The degrees of superheat were in the range of 5 to 20 K. Sun [2] carried out several studies on the ejector refrigeration cycles using 11 different refrigerants. The results showed that the use of R-152a as the working fluid in these systems resulted in higher thermal efficiency than other working fluids. Huang et al. [3] examined three types of solar collectors-- namely those with a flat plate, those with a high efficiency flat plate, and those with vacuum tube collectors-- in the ejector cooling systems. They showed that increasing the collector surface quality, using a good insulation and a glass cover with high performance in flat plate collectors could increase the efficiency and reduce the costs. They used R-141b as the working fluid in solar ejector cooling systems obtaining empirical relations for the efficiency of solar collectors, and they attained a certain temperature range for the cycle best performance. Cizungu et al. [4] accomplished a study on eco-systems and different working fluids such as R-123, R-134a, R-152a, and ammonia. Their results showed that the overall coefficient of performance of the system was dependent on the geometry of ejector and condensation rate. An ejector refrigeration system powered by solar thermal energy was developed by Nguyen et al. [5]. The cooling system was considered passive since there were not any active parts. It was concluded that the ejector efficiency was improved by increasing the pressure difference between the condenser and evaporator. They also designed an experimental system with a nominal cooling capacity of 7 kW and heating capacity of 20 kW. Khattab and Barakat [6] derived the governing equations for each part of the system by studying various components of the ejector refrigeration cycle. They also obtained an expression to predict the cycle cooling capacity on the basis of solar collector efficiency. It was deduced that the coefficient of performance was enhanced by an increase in the evaporator mass flow rate. A decrease in the condenser temperature also yielded a higher coefficient of performance regardless of evaporator and generator temperature. An ejector cooling system assisted by solar energy was modeled in TRNSYS environment by Vidal et al. [7]. The size, area, angle, type, and the hot water mass flow rate of the collector were predicted by this model. They concluded that the annual energy consumption decreased with an increase in the collector area from 20 to 80 m^2. Pridasawas and Lundqvist [8] analyzed and modeled the ejector cooling system with iso-butane (R-600a) as the working fluid using TRNSYS software for an office building. The coefficient of performance of refrigeration cycle, the efficiency of collector, and the area of collector were calculated experimentally in Bangkok. Guo and Shen [9] proposed a lumped method combined with a dynamic model for use in investigating the performance and the solar fraction of a solar-driven ejector refrigeration system using R134a as the working fluid. The results showed that the system could save up to 80% electric energy in comparison with a traditional compressor-based air conditioner when providing the same cooling capacity for office buildings. Numerical and experimental investigation on the system performance of a split-type A/C using an ejector as an expansion device was carried out by Sumeru et al. [10]. The conservation equations of mass, momentum, and energy were applied in the numerical analysis, and it was deduced that the motive nozzle and mixing chamber diameters of 1.1 and 2.5 mm resulted in optimum COP improvement. Smierciew et al. [11] accomplished experimental investigations on a specifically constructed prototype/stand for ejector air conditioning, which operated with isobutane as a working fluid under motive vapor temperature below 75 ˚C. It was concluded that loss coefficient in the investigated set-up was higher than 0.75. Ding et al. [12] proposed an approach to design a two-stage ejector for subzero refrigeration. The generator temperature varied between 63-74 ˚C while the range of evaporator temperature was 24-0 ˚C. They applied the computational fluid dynamics to determine the best

design variables for a range of working conditions. They reported that the suggested two-stage ejector could be used for applications with subzero refrigeration. Zhang et al. [13] studied the feasibility of using an ejector in an organic Rankine cycle and an ejector refrigeration cycle. They tried to find an optimum distance for the nozzle position to have the highest entrainment ratio, the lowest loss in the ejector, and the best efficiency. They reported that the evaporator conditions such as pressure, temperature, and flow rate could considerably affect the coefficient of performance (COP) and entrainment ratio. Liu et al. [14] proposed a simple model to evaluate the ejector performance in a refrigeration system. They applied the traditional identification methods to determine the unknown parameters of the proposed model. The results showed that the ejector entrainment ratio and the critical back pressure could be predicted by the suggested model accurately. Hou et al. [15] simulated a parallel hybrid ejector-based refrigerator-freezer cooling cycle to obtain optimum ejector geometric parameters. They also investigated the effect of blocking percentage of nozzle on the performance of ejector. They reported that blocking percentage of primary nozzle on the ejector performance was significant. Kitrattana et al. [16] tested a steam ejector designed based on the constant rate of momentum change (CRMC) to compare its performance with that of a traditional ejector. They also designed three different ejectors to evaluate CRMC ejector. They concluded that entrainment ratio of CRMC ejector was higher than that of the traditional ejectors while the ejector area ratio, the critical condenser pressure, and operating conditions were supposed to be the same. Liu et al. [17] improved the performance of a conventional ejector cooling cycle by applying a flash tank economizer and an auxiliary ejector. The proposed cooling cycle had the capability to enhance the overall entrainment ratio of the ejectors, cooling capacity of the cycle, and the coefficient of performance by decreasing the flash gas entered into the evaporator. The results showed that the performance of the proposed cooling cycle was better than that of a conventional ejector cooling cycle under a higher evaporating temperature. Kumar and Sachdeva [18] introduced a novel 1-D mathematical model to determine complete geometry of an ejector. The area ratios predicted by the mathematical model were compared with those of the experimental/numerical results presented in the literature, and they reported that they were in good agreement. They also validated the proposed model with a CFD analysis and they concluded that average deviation in the entrainment ratio was about 2.48 %. Mohammadi [19] investigated the geometrical factors of multi-stage stream ejectors using computational fluid dynamics. The effects of various parameters including the diameters of the nozzle, the throat, the mixing chamber, and nozzle exit position were studied, and suitable values were obtained to have proper functioning of each stage, the entrainment and compression ratio. He also analyzed the pressure contour and the Mach number for the final geometry of the ejectors. Chen et al. [20] studied the ejector cooling cycles with the heat-driven feed pumping devices which provided the working fluid to a vapor generator. The working fluid of the ejector cooling cycles was supposed to be R245ca due to its compatibility with the environment. The influence of generating and condensing temperature on the behavior of ejector cooling cycles was also investigated. They also evaluated the energy and exergy efficiency of the suggested cycles. Nguyen et al. [21] investigated the effects of a variable geometry ejector design on the characteristic of a solar heat driven ejector cooling cycle under real-life working conditions experimentally. The effects of the area ratio and the nozzle exit position on the cooling cycle performance were investigated. They concluded that the coefficient of performance increased by 24% for the cooling cycle with variable geometry ejector in comparison with the cycle with a fixed geometry ejector. Zhang et al. [22] introduced a new type of ocean thermal energy conversion with two ammonia ejectors to improve the system efficiency. They studied the influence of geometrical parameters and working pressures on the vapor-vapor ammonia ejectors numerically. They concluded that thermal efficiency of the new ocean thermal energy conversion increased by 10.33% compared to the cycle without the ejectors. Ruangtrakoon and Thongtip [23] accomplished some experiments on the R141b ejector refrigeration system to investigate the influence of the generator temperature on the ejector performance under various working conditions. They varied the generator temperature to obtain the optimal generator temperature. They concluded that the optimal generator temperature was a function of the working conditions and primary nozzle used.

In this paper, the feasibility study and an analysis of a solar ejector cooling cycle in different climatic regions are conducted. The thermodynamic analysis of an ejector

[DOR: 20.1001.1.23452951.1400.11.4.2.1]
[DOI: 10.22052.11.4.60]

cooling cycle is explained in detail. Next, the intensity of solar radiation on the surface perpendicular to the beam of the sun in the low-dust air condition is calculated. Furthermore, the effects of operating conditions-- namely the generator, condenser, and evaporator temperatures-- on the system performance are also investigated. Based on weather conditions in different regions, the performance of the ejector cooling cycle in several months of the year will be determined. This type of system is used to reduce the cycle energy consumption by using solar energy. Furthermore, the elimination of compressor causes considerable savings in maintenance and investment costs.

2. Ejector Refrigeration Cycle

The ejector refrigeration cycle is shown in Fig. 1, where the compressor is replaced by an ejector and a solar thermal source.

The refrigerant pumped into the generator will be evaporated after receiving heat, and, then, it will enter the ejector. The speed of refrigerant will increase, and its pressure will decrease when flowing through the ejector nozzle. The pressure at the exit of ejector nozzle is, thus, less than the evaporator pressure. The low pressure at the top of evaporator will bring up the vapor from the evaporator and mix it with the vapor at the nozzle exit (suction chamber). The vapor from the suction chamber enters the diffuser at the condenser entrance. The vapor changes phase by giving heat to the environment. A portion of liquid refrigerant enters the generator, and the rest will pass through the throttle valve entering the evaporator.

The schematic diagram of the ejector cooling cycle is shown in Fig. 2.

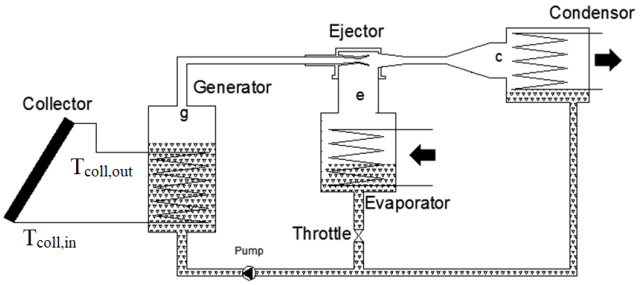

Fig. 1: Solar driven ejector refrigeration system

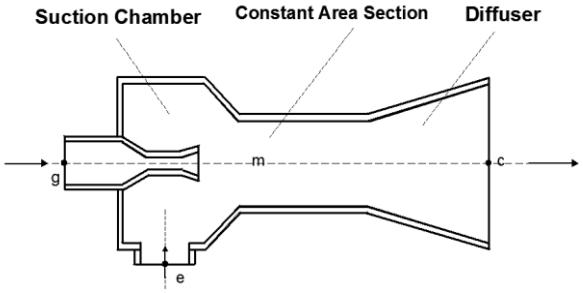

Fig. 2: Details of ejector

3. The Governing Equations

The ejector cooling cycle analyzed in this study together with its subsystems is shown in a pressure-enthalpy diagram in Fig. 3. The governing equations of this cycle are similar to those of the compression refrigeration cycles, and only specific equations are derived for the ejector. The energy balance at the mixing point of the ejector can be written as:

$$(m_g + m_e)h_5 = m_e h_9 + m_g h_3 \quad (1)$$

The momentum conservation law at the mixing section of the ejector yields:

$$m_g c_g + m_e c_e = (m_g + m_e)c_m \quad (2)$$

Assuming that the inlet area of the evaporator is large enough, the inlet velocity c_e can be set to zero; thus, Eq. 2 is simplified:

$$\frac{m_e}{m_g} = \frac{c_g}{c_m} - 1 \quad (3)$$

The nozzle's isentropic efficiency (η_N) is defined as:

$$\eta_N = \frac{h_3 - h_4}{h_3 - h_{4,iso}} \quad (4)$$

Based on the energy conservation equation, the velocity of the stream at the nozzle exit (c_g) can be expressed as follows with the assumption of adiabatic conditions, of no external work, and of no elevation change (z_B=z_A):

$$c_g = \sqrt{2(h_3 - h_4)} = \sqrt{2(\eta_N)(h_3 - h_{4,iso})} \quad (5)$$

The diffuser isentropic efficiency (η_D) is defined as:

$$\eta_N = \frac{h_3 - h_4}{h_3 - h_{4,iso}} \quad (6)$$

The pressure of the mixed flow at the nozzle entrance (point 5 in Fig. 3) is higher than the pressure values at points 4 and 9. The velocity of the mixed flow can be

expressed as:

$$c_m = \sqrt{2(h_6 - h_5)} = \sqrt{2(1/\eta_D)(h_{6,iso} - h_5)} \quad (7)$$

Inserting Eqs. 5 and 7 into Eq. 3 gives:

$$\omega = \frac{m_e}{m_g} = \sqrt{(\eta_N \eta_D)\left(\frac{h_3 - h_{4,iso}}{h_{6,iso} - h_5}\right)} - 1 \quad (8)$$

The product of the isentropic efficiency of the nozzle (η_N) and the isentropic efficiency of the diffuser (η_D) will result in ejector isentropic efficiency (λ):

$$\lambda = \eta_N . \eta_D \quad (9)$$

Neglecting the pump input work, the thermal COP of the ejector refrigeration system is defined as the ratio of cooling capacity and input heat to the generator [24]:

$$Cop = \frac{Q_e}{Q_g} \quad (10)$$

It can also be expressed as follows:

$$COP = \frac{m_e(h_9 - h_8)}{m_g(h_3 - h_1)} \quad (11)$$

The following assumptions are made to solve the above equations:

1. The fluid at the exit of generator and evaporator as well as the fluid at the input of the condenser are at the state of saturated steam.

2. In order to generate a suction pressure in the suction chamber, the temperature at point 5 is supposed to be 5 degrees less than the evaporator temperature, and its state is saturated steam.

3. The fluid at condenser outlet is a condensed liquid with 5 degrees cooler than its inlet temperature.

4. The efficiency of the ejector is assumed to be 0.7.

5. The cooling capacity of the system is supposed to be 3.5 kW.

According to the preceding assumptions, the governing equations are solved in EES software. The following equations are also used in the feasibility study of the cooling ejector cycle.

The intensity of solar radiation on the surface perpendicular to the beam of the sun in the low-dust air condition is calculated as follows [25]:

$$I(\theta_z) = 81.738\,[1 - \exp(-0.75(90 - \theta_z))] \quad (12)$$

where θ_z is the angle between the beam of the sun and the normal to the horizontal surface. Considering the effect of clouds in the sky, the equation of direct radiation on a horizontal surface will be as follows:

$$G_v = I(\theta_Z)\cos\theta_z(1 - CF) \quad (13)$$

To determine the amount of scattered radiation on a horizontal surface, one can write [25]:

$$D(\theta_z, CF) = 0.123 + 0.181(90 - \theta_z) + 10.43CF \quad (14)$$

The CF in above formulas is monthly cloud factor.

The schematic diagram of a solar collector with solar angles is displayed in Fig. 4. The angle between the radiation beam and the vector perpendicular to the surface is obtained from the following equation [26]:

$$\begin{aligned}\cos\theta &= \sin\delta\sin\phi\cos\beta \\ &- \sin\delta\cos\phi\sin\beta\cos\gamma \\ &+ \cos\delta\cos\phi\cos\beta\cos\omega \\ &+ \cos\delta\sin\phi\sin\beta\cos\gamma\cos\omega \\ &+ \cos\delta\sin\beta\sin\gamma\sin\omega\end{aligned} \quad (15)$$

Where **φ** is the latitude of different Iranian cities in radians, β is the angle of solar collector with the horizontal surface, γ is deviation angle from the north to the south, ω is deviation angle of solar collector from the west to the east. And δ is the deviation angle of the sun from the earth obtained from the following equation [27]:

$$\delta = 23.45\sin\left(360\frac{284 + n}{365}\right) \quad (16)$$

In the above equation, *n* is the number of days starting from January the first. In this study, *n* is used for the mid-day of the month. The average value of n for days of every month is presented in Ref. [15]. The amounts of β (monthly optimum angle), ω, and γ are considered 30, 0, and 0 degrees respectively.

To calculate the intensity of reflected beam from the earth, the following relation is used [26]:

$$G_r = I(\theta_z)\rho_g\left(\frac{1 - \cos\beta}{2}\right) \quad (17)$$

where ρ_g is the coefficient of the reflection of light from the ground. In this study, it is assumed to be 0.2. The amount of the solar radiation received by the collector is calculated from the following equation:

$$G = 41870 \times (G_r + G_v + D)/3600 \quad (18)$$

Data represented in Table 1 are used to determine the cloud factor [25]:

Based on Table 1, Cloud factors depends highly on the location of each city (latitude) and the selected month. Based on Table 1, the cloud factor is maximum in July for Chabahar, while this parameter is minimum in

[DOR: 20.1001.1.23452951.1400.11.4.2.1]
[DOI: 10.22052.11.4.60]

October. For Rasht, Ramsar, and Babolsar cloud factor is minimum in July, while the maximum value of the cloud factor for these cities occurs in March. Rasht, Ramsar, and Babolsar are located in higher latitude, while Chabahar is in lower latitude.

To determine the temperature at different hours of a day, the following equation is used [28]:

$$T_{\infty,t} = \frac{1}{2}(T_{max} + T_{min}) + \frac{1}{2}(T_{max} - T_{min}) \times Cos[\frac{\Pi}{12}(t - t_{max})] \quad (19)$$

where T_{max} and T_{min} are the maximum and minimum temperature in a day; t and t_{max} are the selected time and the time at which the maximum temperature occurs. They has been considered 12 p.m. and 14 p.m. respectively in this paper. Maximum and minimum temperatures in Eq. 19 for various cities in Iran are determined using meteorological data.

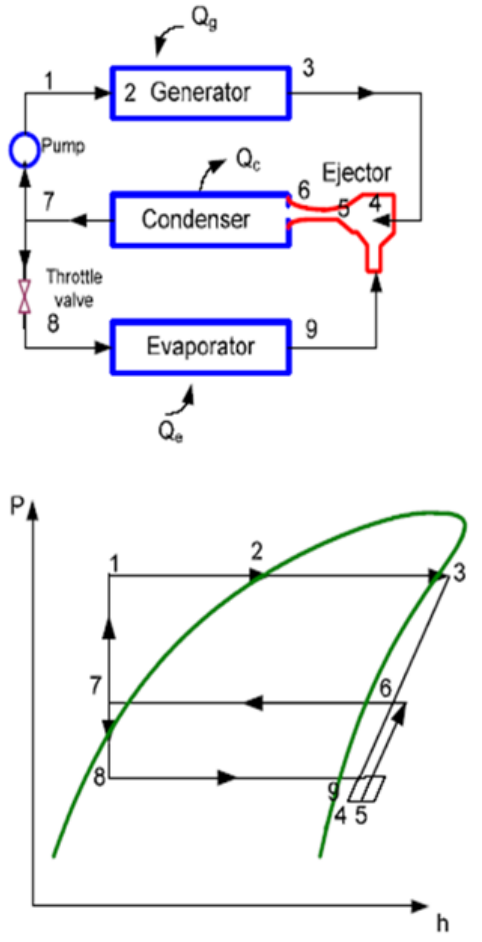

Fig. 3: Schematic diagram of an ejector refrigeration cycle in P-h diagram

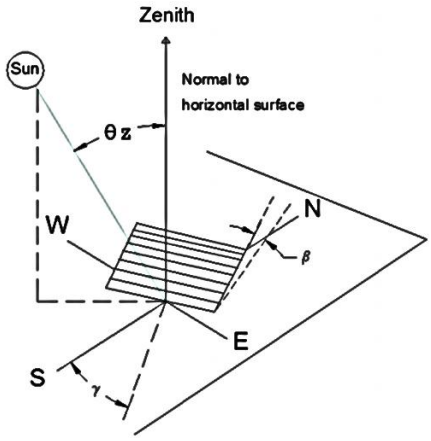

Fig. 4: A schematic of solar collector with illustrative angles [26]

4. Results and Discussions

To determine the coefficient of performance of the solar ejector cooling cycle, we used different fluids as the working fluid. These fluids include R113, R114, R600, R600a, and R141b, which are commonly used in the refrigeration cycles.

The effect of generator temperature on the COP for various working fluids is investigated at constant evaporator and condenser temperature which are considered to be 10 and 35 °C respectively. The results show that increasing the temperature of fluid at exit of the generator yields higher COP for the selected working fluids. Since the cooling capacity and evaporator temperature were assumed to be constant, it can be deduced that increasing the generator temperature will lead to lower mass flow rate from the condenser to the generator.

To obtain higher generator temperature, the generator pressure should be increased; this is not recommended from an economical point of view. Due to decreasing the mass flow rate at the generator input, increasing the generator temperature has a positive effect on improving COP. The variation of COP versus generator temperature is illustrated in Fig. 5. The rate of increase in COP, when the generator temperature varies in the range of 80-100 °C, is about 40%, while this rate of increase in the range of 100-120 °C is only 21%.

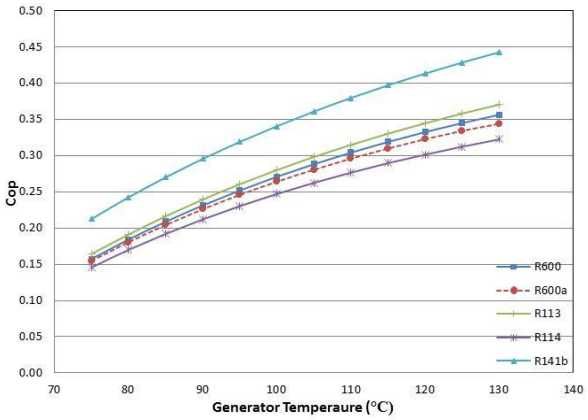

Fig. 5: The effect of generator temperature on COP for selected working fluids

The effect of condenser temperature on the COP for various working fluids is shown in Fig. 6. In this figure the generator and evaporator temperatures are assumed to be 120°C and 10°Crespectively, and the cooling capacity is 3.5 kW. Based on Fig., 6 it is observed that rising condenser temperature causes a dramatic decrease in COP. This is true for selected working fluids. It is clear that an increase in ambient temperature has a significant effect on the working conditions of these systems. In other words, these systems are less efficient in the warmer environment than in that environment with low temperature. The reduction of COP is about 10% in the range of 27-29°C for the condenser temperature. It is noticeable that the rate of COP reduction at various condenser temperature remains constant.

The effects of evaporator temperatures on COP for various working fluids-- when the cooling capacity, generator, and condenser temperature are assumed 3.5 kW, 120 and 35°C respectively-- are illustrated in Fig. 7.

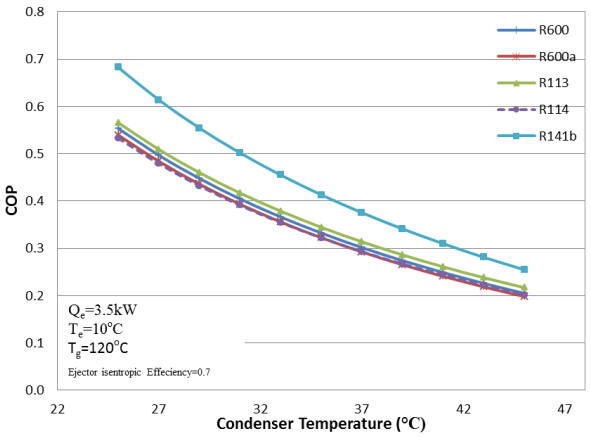

Fig. 6: Effect of condensing temperature on COP for selected refrigerants

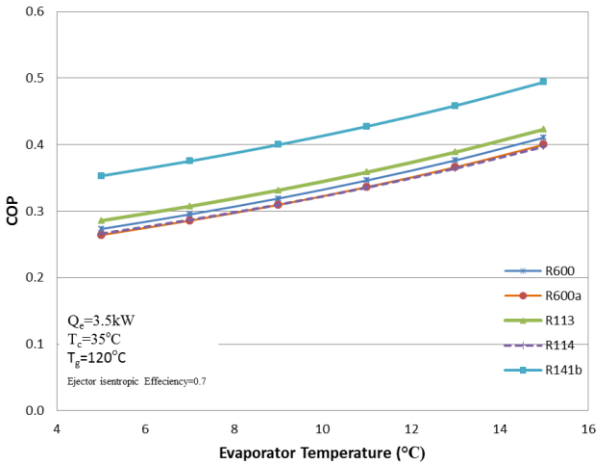

Fig. 7: COP of an ejector refrigeration cycle as a function of evaporator temperature for selected working fluids

The results show that increasing the fluid temperature at the exit of the evaporator increases COP for the selected working fluids. The results also suggest that an increase in evaporator temperature has a minor effect on the mass flow rate through the evaporator. It should be mentioned that the performance of these systems strongly depends on the initial temperature of the place that is supposed to be cooled. At higher initial temperature, COP will be improved, while at lower temperature its performance will be deteriorated. Studies show that the rates of COP increase for the evaporator temperature ranges of 13-15°C and 7-9°C are about 8 and 6% respectively. To determine COP in different cities, generator temperature and evaporator temperature were assumed to be constant (125 and 10°C respectively), while the condenser temperature was varied. Since a wide range of condenser temperature was selected for various ambient temperatures, an expression was proposed on the basis of various available temperatures and statistical methods to facilitate the process of calculating COP.

$$COP = a\left(\frac{T_c - T_e}{T_g - T_e}\right)^b + c \qquad (20)$$

After calculating a, b, and c from statistical methods, Eq. 20 results in:

$$COP = 0.9769 - 1.68634\left(\frac{T_c - T_e}{T_g - T_e}\right)^{0.6604} \qquad (21)$$

As shown in Fig. 8 and Table 2, the data obtained from Eq. 21 are in close agreement with those deduced from EES software.

[DOR: 20.1001.1.23452951.1400.11.4.2.1]
[DOI: 10.22052.11.4.60]

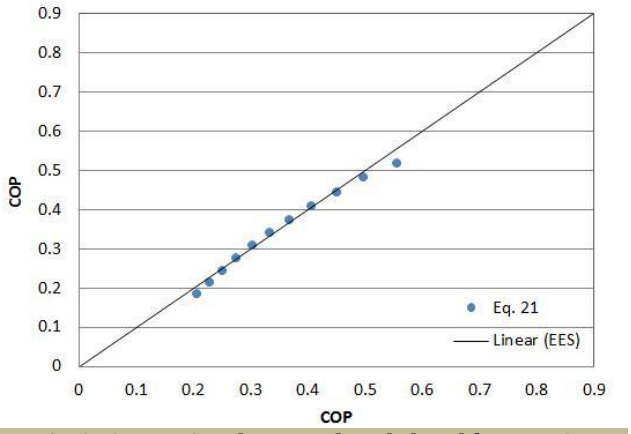

Fig. 8: Comparison between data deduced from EES software and those inferred from Eq. 21 at Te=10 °C and Tg=125 °C

Tables 3 to 6 show the solar radiation intensity, COP, and the collector area for various Iranian cities in different months of the year, while the cooling capacity is supposed to be 1 kW. Based on Tables 3 to 6, the collector area is increased as ambient temperature enhances because increasing the condenser temperature leads to lower COP. Since the cooling capacity was supposed to be constant, Q_g will increase, and it means that a higher collector area is necessary to provide such a heat duty. In some cities, although smaller collector area is required in comparison with other cities, but these cities benefit from higher solar radiation intensity compensating the required generator energy.

Table 1: Cloud factors for selected months in different Iranian cities [14]

No	City	φ	Mar	Apr	May	Jun	Jul	Aug	Sept	Oct
1	**Rasht**	37.20	0.79	0.672	0.514	0.54	0.5	0.573	0.605	0.625
2	**Ramsar**	36.90	0.753	0.667	0.579	0.545	0.526	0.614	0.656	0.678
3	**Babolsar**	36.72	0.649	0.591	0.484	0.436	0.434	0.483	0.531	0.542
4	**Tabriz**	38.83	0.528	0.5	0.379	0.198	0.192	0.178	0.183	0.304
5	**Oromiyeh**	37.53	0.563	0.51	0.389	0.205	0.176	0.152	0.201	0.337
6	**Tehran**	35.68	0.456	0.4	0.352	0.209	0.216	0.186	0.18	0.242
7	**Hamedan**	34.85	0.501	0.502	0.387	0.194	0.214	0.201	0.226	0.297
8	**Kermanshah**	34.28	0.486	0.477	0.359	0.157	0.168	0.166	0.181	0.291
9	**Kashan**	33.98	0.497	0.482	0.431	0.43	0.38	0.292	0.268	0.37
10	**Khoramabad**	33.48	0.465	0.478	0.35	0.184	0.187	0.193	0.194	0.212
11	**Shahrekord**	32.33	0.392	0.441	0.282	0.208	0.243	0.191	0.151	0.173
12	**Mashhad**	36.27	0.591	0.499	0.343	0.188	0.174	0.142	0.171	0.265
13	**Semnan**	35.55	0.453	0.43	0.358	0.246	0.226	0.184	0.186	0.229
14	**Birjand**	35.87	0.398	0.384	0.294	0.207	0.18	0.158	0.127	0.145
15	**Esfehan**	32.62	0.299	0.349	0.32	0.162	0.206	0.168	0.149	0.159
16	**Yazd**	31.90	0.379	0.423	0.338	0.274	0.241	0.164	0.141	0.148
17	**Ahvaz**	31.33	0.465	0.457	0.379	0.267	0.266	0.217	0.177	0.258
18	**Abadan**	30.37	0.36	0.398	0.347	0.258	0.262	0.232	0.185	0.228
19	**Kermanshah**	30.25	0.359	0.435	0.297	0.244	0.235	0.207	0.192	0.219
20	**Shiraz**	29.60	0.347	0.381	0.223	0.147	0.195	0.184	0.131	0.13
21	**Zahedan**	29.47	0.403	0.409	0.317	0.264	0.257	0.201	0.171	0.203
22	**Boushehr**	28.98	0.337	0.366	0.26	0.182	0.216	0.2	0.168	0.168
23	**Bandar Abbas**	27.22	0.353	0.354	0.212	0.254	0.357	0.299	0.251	0.176
24	**Chabahar**	25.28	0.262	0.249	0.215	0.314	0.373	0.382	0.291	0.165

[DOR: 20.1001.1.23452951.1400.11.4.2.1]
[DOI: 10.22052.11.4.60]

Table 2: Comparison between data deduced from EES software and those inferred from Eq. 21 at T_e=10 °C and T_g=125 °C

T_c (°C)	m_g(kg.s^{-1})	m_e(kg.s^{-1})	ω	Q_e (kW)	Q_g (kW)	COP	Correlation
25	0.013	0.010	0.793	3.50	6.33	0.55	0.52
27	0.014	0.010	0.715	3.50	7.05	0.50	0.49
29	0.016	0.010	0.647	3.50	7.82	0.45	0.45
31	0.018	0.104	5.871	3.50	8.65	0.40	0.41
33	0.020	0.011	0.535	3.50	9.55	0.37	0.38
35	0.022	0.011	0.487	3.50	10.53	0.33	0.34
37	0.024	0.011	0.444	3.50	11.60	0.30	0.31
39	0.027	0.011	0.406	3.50	12.77	0.27	0.28
41	0.303	0.011	0.037	3.50	14.06	0.25	0.25
43	0.034	0.011	0.338	3.50	15.49	0.23	0.22
45	0.038	0.012	0.308	3.50	17.08	0.20	0.19

Table 3: collector area, coefficient of performance, and solar radiation intensity for various Iranian cities in April

				April		
No.	**City**	**φ**	**T(°C)**	**G(W.m^{-2})**	**COP**	**A(m^2)**
1	**Rasht**	37.20	18.46	452.00	0.45	8.92
2	**Ramsar**	36.90	16.06	456.09	0.44	8.18
3	**Babolsar**	36.72	17.64	523.99	0.49	6.76
4	**Tabriz**	38.83	16.16	608.36	0.53	5.11
5	**Oromiyeh**	37.53	16.02	597.76	0.53	5.23
6	**Tehran**	35.68	21.37	693.56	0.58	5.03
7	**Hamedan**	34.85	17.37	600.80	0.53	5.41
8	**Kermanshah**	34.28	19.11	622.13	0.54	5.44
9	**Kashan**	33.98	25.35	617.09	0.56	6.86
10	**Khoramabad**	33.48	21.63	619.69	0.55	5.96
11	**Shahrekord**	32.33	17.62	650.24	0.55	4.86
12	**Mashhad**	36.27	19.96	605.81	0.54	5.82
13	**Semnan**	35.55	23.10	666.46	0.57	5.66
14	**Birjand**	35.87	23.69	708.21	0.59	5.31
15	**Esfehan**	32.62	21.80	732.84	0.59	4.74
16	**Yazd**	31.90	25.56	665.26	0.58	6.22
17	**Ahvaz**	31.33	31.12	633.70	0.58	8.42
18	**Abadan**	30.37	31.91	683.58	0.60	7.88
19	**Kerman**	30.25	23.22	650.50	0.57	5.88
20	**Shiraz**	29.60	23.09	696.48	0.58	5.32
21	**Zahedan**	29.47	26.67	671.36	0.58	6.41
22	**Boushehr**	28.98	28.88	707.89	0.60	6.54
23	**Bandar Abbas**	27.22	31.17	712.72	0.60	7.20
24	**Chabahar**	25.28	30.16	796.90	0.62	5.93

[DOR: 20.1001.1.23452951.1400.11.4.2.1]
[DOI: 10.22052.11.4.60]

Table 4: collector area, coefficient of performance, and solar radiation intensity for various Iranian cities in May and June

			May				June			
No.	**City**	**φ**	**T(°C)**	**G(W.m^{-2})**	**COP**	**A(m^2)**	**T(°C)**	**G(W.m^{-2})**	**COP**	**A(m^2)**
1	**Rasht**	37.20	23.44	574.24	0.54	7.10	27.33	538.67	0.53	9.05
2	**Ramsar**	36.90	20.96	516.42	0.50	7.69	25.34	533.40	0.52	8.51
3	**Babolsar**	36.72	22.82	599.17	0.54	6.52	27.20	626.30	0.57	7.22
4	**Tabriz**	38.83	21.89	697.76	0.58	5.08	27.80	840.50	0.63	4.99
5	**Oromiyeh**	37.53	21.32	685.02	0.57	5.11	26.52	828.43	0.62	4.82
6	**Tehran**	35.68	27.11	711.19	0.59	6.04	33.03	815.80	0.63	6.62
7	**Hamedan**	34.85	22.32	677.70	0.57	5.37	28.77	824.11	0.63	5.34
8	**Kermanshah**	34.28	25.00	699.88	0.59	5.68	32.14	852.25	0.64	5.99
9	**Kashan**	33.98	30.80	636.42	0.58	8.25	37.11	620.25	0.59	11.98
10	**Khoramabad**	33.48	27.74	704.50	0.59	6.28	34.53	824.83	0.64	7.08
11	**Shahrekord**	32.33	23.43	758.02	0.60	4.80	29.70	797.94	0.62	5.80
12	**Mashhad**	36.27	25.64	721.13	0.59	5.59	31.13	836.75	0.63	5.83
13	**Semnan**	35.55	28.58	705.48	0.60	6.49	34.36	783.58	0.63	7.49
14	**Birjand**	35.87	29.19	762.48	0.61	6.01	33.85	818.45	0.63	6.89
15	**Esfehan**	32.62	27.23	726.68	0.60	5.89	33.24	838.05	0.64	6.47
16	**Yazd**	31.90	31.12	708.11	0.60	7.24	36.66	740.48	0.62	9.21
17	**Ahvaz**	31.33	38.09	670.63	0.61	11.50	43.23	743.03	0.64	15.39
18	**Abadan**	30.37	38.57	693.49	0.61	11.37	42.66	744.68	0.63	14.50
19	**Kerman**	30.25	28.71	735.27	0.60	6.18	33.64	755.45	0.62	7.55
20	**Shiraz**	29.60	29.37	794.37	0.62	5.75	34.77	830.47	0.64	7.12
21	**Zahedan**	29.47	31.41	714.47	0.60	7.25	35.03	734.21	0.62	8.46
22	**Boushehr**	28.98	33.76	759.87	0.62	7.54	35.72	797.68	0.63	7.91
23	**Bandar Abbas**	27.22	35.72	789.66	0.63	8.02	37.90	727.57	0.62	10.20
24	**Chabahar**	25.28	32.98	774.90	0.62	7.05	34.08	667.02	0.60	9.10

[DOR: 20.1001.1.23452951.1400.11.4.2.1]
[DOI: 10.22052.11.4.60]

Table 5: collector area, coefficient of performance, and solar radiation intensity for various Iranian cities in July and August

			July				August			
No.	**City**	**φ**	**T(°C)**	**G(W.m^{-2})**	**COP**	**A(m^2)**	**T(°C)**	**G(W.m^{-2})**	**COP**	**A(m^2)**
1	**Rasht**	37.20	30.30	579.36	0.55	8.93	29.44	534.19	0.53	9.99
2	**Ramsar**	36.90	28.60	555.86	0.54	8.91	28.24	497.08	0.51	10.62
3	**Babolsar**	36.72	30.30	635.01	0.58	7.89	29.96	613.45	0.57	8.35
4	**Tabriz**	38.83	32.70	853.85	0.64	5.88	31.69	890.41	0.64	5.54
5	**Oromiyeh**	37.53	31.20	862.29	0.64	5.38	29.99	910.54	0.64	4.97
6	**Tehran**	35.68	36.60	819.19	0.64	7.66	34.78	875.12	0.65	6.67
7	**Hamedan**	34.85	34.20	816.90	0.63	6.55	32.67	859.27	0.64	6.09
8	**Kermanshah**	34.28	37.90	853.42	0.64	7.61	35.95	888.44	0.65	7.01
9	**Kashan**	33.98	40.80	670.85	0.61	12.92	38.79	775.99	0.63	10.00
10	**Khoramabad**	33.48	39.60	832.95	0.64	8.81	37.92	861.83	0.65	8.26
11	**Shahrekord**	32.33	33.90	779.30	0.62	6.86	31.93	859.42	0.64	5.86
12	**Mashhad**	36.27	34.40	858.21	0.64	6.31	31.87	915.97	0.65	5.40
13	**Semnan**	35.55	37.70	809.95	0.64	8.33	35.95	876.50	0.65	7.13
14	**Birjand**	35.87	35.70	851.11	0.64	6.85	33.33	900.56	0.65	5.95
15	**Esfehan**	32.62	36.70	812.12	0.63	7.70	34.49	880.72	0.65	6.51
16	**Yazd**	31.90	39.40	778.66	0.63	9.68	36.92	881.47	0.65	7.52
17	**Ahvaz**	31.33	46.30	754.56	0.64	18.56	44.55	832.76	0.66	15.43
18	**Abadan**	30.37	46.90	752.55	0.64	19.97	44.19	815.78	0.65	15.19
19	**Kerman**	30.25	35.70	774.36	0.62	7.66	32.99	837.10	0.64	6.40
20	**Shiraz**	29.60	37.80	803.64	0.64	8.29	35.83	854.30	0.64	7.31
21	**Zahedan**	29.47	37.00	751.50	0.62	8.61	34.57	838.94	0.64	6.95
22	**Boushehr**	28.98	37.90	782.42	0.63	8.92	37.44	837.64	0.64	8.28
23	**Bandar Abbas**	27.22	38.30	656.48	0.60	11.58	37.11	744.27	0.62	9.41
24	**Chabahar**	25.28	33.20	632.40	0.58	9.19	31.57	664.80	0.59	8.05

[DOR: 20.1001.1.23452951.1400.11.4.2.1]
[DOI: 10.22052.11.4.60]

Table 6: collector area, coefficient of performance, and solar radiation intensity for various Iranian cities in September and October

			September				October			
No.	**City**	**φ**	**T(°C)**	**G(W.m^{-2})**	**COP**	**A(m^2)**	**T(°C)**	**G(W.m^{-2})**	**COP**	**A(m^2)**
1	**Rasht**	37.20	26.08	507.47	0.51	9.46	21.40	461.57	0.46	9.41
2	**Ramsar**	36.90	25.28	462.43	0.48	10.68	21.14	417.23	0.43	11.19
3	**Babolsar**	36.72	27.16	574.44	0.54	8.17	22.44	533.96	0.51	7.67
4	**Tabriz**	38.83	27.28	879.94	0.63	4.61	19.68	727.13	0.58	4.44
5	**Oromiyeh**	37.53	26.05	867.39	0.63	4.46	19.20	705.46	0.58	4.56
6	**Tehran**	35.68	30.78	890.42	0.64	5.30	23.66	795.31	0.61	4.54
7	**Hamedan**	34.85	27.93	850.87	0.63	4.94	20.31	751.65	0.59	4.34
8	**Kermanshah**	34.28	31.33	892.22	0.64	5.44	24.23	759.22	0.60	4.94
9	**Kashan**	33.98	34.17	814.71	0.63	7.05	26.59	691.94	0.59	6.13
10	**Khoramabad**	33.48	33.68	881.88	0.64	6.22	26.78	831.17	0.62	4.85
11	**Shahrekord**	32.33	28.24	922.10	0.64	4.53	21.59	870.07	0.62	3.75
12	**Mashhad**	36.27	27.73	897.21	0.64	4.58	21.21	772.82	0.60	4.32
13	**Semnan**	35.55	31.84	885.33	0.64	5.63	24.42	807.12	0.61	4.59
14	**Birjand**	35.87	30.49	937.47	0.65	4.91	25.21	877.75	0.63	4.25
15	**Esfehan**	32.62	30.65	923.52	0.65	5.04	23.92	881.09	0.63	4.02
16	**Yazd**	31.90	33.17	930.91	0.65	5.66	26.51	893.75	0.63	4.37
17	**Ahvaz**	31.33	41.20	897.92	0.66	10.07	34.73	799.55	0.63	7.45
18	**Abadan**	30.37	42.69	889.39	0.66	11.68	34.83	829.40	0.64	7.15
19	**Kerman**	30.25	30.10	882.94	0.64	5.19	24.63	837.74	0.62	4.41
20	**Shiraz**	29.60	32.45	936.59	0.65	5.41	26.68	918.59	0.64	4.26
21	**Zahedan**	29.47	31.18	900.49	0.64	5.33	26.50	854.58	0.63	4.63
22	**Boushehr**	28.98	35.72	902.31	0.65	6.79	32.08	887.16	0.64	5.68
23	**Bandar Abbas**	27.22	36.10	824.43	0.64	7.77	34.15	885.63	0.65	6.35
24	**Chabahar**	25.28	31.30	784.18	0.62	6.39	31.40	900.65	0.64	5.39

5. Conclusions

The thermodynamic analysis of an ejector cooling cycle, assisted by solar energy, is accomplished in this paper. Based on the obtained results, COP will increase as generator temperature and evaporator temperature enhance, and condenser temperature decreases. Therefore, condenser temperature must be kept low

[DOR: 20.1001.1.23452951.1400.11.4.2.1]
[DOI: 10.22052.11.4.60]

enough to increase the system performance. For selected refrigerants, the ejector cooling system is more efficient at higher evaporator temperature. The results show that in lower generator temperature ranges, the variation of COP versus generator temperature is more than that at higher generator temperature ranges. In other words, the slope of COP versus T_g curve decreases as generator temperature increases. Furthermore, the slope of COP versus T_c curve remains approximately constant at various condenser temperature ranges. Feasibility study of a solar ejector cooling cycle is accomplished to determine the collector area as a main factor for each Iranian city. The results show a smaller collector area is required for cities with higher ambient temperature. Sometimes increasing the collector area in cities with lower ambient temperature may not be economical, and, as a result, a solar ejector cooling cycle is not recommended. Combining the solar ejector cooling cycle with absorption cycle can improve its efficiency and feasibility of this combined cycle for various weather conditions in Iran can be achieved as the future task. Furthermore, exergy analysis and minimizing the entropy generation of the combined cycle can also be considered other constructive suggestions for future studies.

Nomenclature

c_e(m s^{-1}): Velocity of the entrained (secondary) refrigerant from the evaporator
c_g(m s^{-1}): Velocity of the primary fluid from the generator, expanded through the nozzle in the ejector
c_m(m s^{-1}): Velocity of the mixed fluid leaving the mixing section
COP: Coefficient of Performance of the ejector
CF: Cloud Factor
D(Cal/cm^2.hr): Scattered radiation on a horizontal surface
G(W m^{-2}): Solar flux density, solar energy irradiation
h(kJ kg^{-1}): Enthalpy
n: number of day
m(kg s^{-1}): Mass flow rate
m_e(kg s^{-1}): Mass flow rate of the entrained refrigerant from the evaporator
m_g(kg s^{-1}): Mass flow rate of driving fluid from generator
Q(kW): Heat transfer rate
t(s): time
T(°C): Temperature
T_g(°C): Generator temperature
T_e(°C): Evaporator temperature
$T_{\infty,t}$(°C): Ambient temperature
z(m): Height

Greeks Alphabets:

η_N: Nozzle efficiency
η_D: Diffuser efficiency
δ: Angle deviation of the sun from earth
ω: Angle deviation of solar collector from west to east
γ: Angle deviation from north to south
φ: Latitude of different areas of the country
β: Angle of solar collector with the horizontal solar collector
θ_z: Angle between the beam of the sun and the perpendicular line to the horizontal surface

Subscripts:

c: Condenser
e: Evaporator
D: Diffuser
g: Generator
max: Maximum
min: Minimum
N: Nozzle
iso: Isentropic

References

[1] Huang, B.J., Chang, J.M., Wang, C.P. and Petrenko V.A., "A 1-D analysis of ejector performance", Int. J. Refrig., Vol. 22, pp. 354–364, 1999.

[2] Sun, D.-W., "Comparative study of the performance of an ejector refrigeration cycle operating with various refrigerants", Energy Convers. Manag., Vol. 40, pp. 873–884, 1999.

[3] Huang, B.J., Petrenko, V.A., Samofatov, I.Y. and Shchetinina, N.A., "Collector selection for solar ejector cooling system", Sol. Energy., Vol. 71, pp. 269–274, 2001.

[4] Cizungu, K., Mani, A. and Groll, M., "Performance comparison of vapour jet refrigeration system with environment friendly working fluids", Appl. Therm. Eng., Vol. 21, pp. 585–598, 2001.

[5] Nguyen, V.M., Riffat, S.B. and Doherty P.S., "Development of a solar-powered passive ejector cooling system", Appl. Therm. Eng., Vol. 21, pp. 157–168, 2001.

[6] Khattab, N.M. and Barakat M.H., "Modeling the design and performance characteristics of solar steam-jet cooling for comfort air conditioning", Sol. Energy., Vol. 73, pp. 257–267, 2002.

[7] Vidal, H., Colle, S. and Pereira, G.D.S., "Modelling

[DOR: 20.1001.1.23452951.1400.11.4.2.1]
[DOI: 10.22052.11.4.60]

and hourly simulation of a solar ejector cooling system", Appl. Therm. Eng., Vol. 26, pp. 663–672, 2006.

[8] Pridasawas, W. and Lundqvist, P., "A year-round dynamic simulation of a solar-driven ejector refrigeration system with iso-butane as a refrigerant", Int. J. Refrig., Vol. 30, pp. 840–850, 2007.

[9] Guo, J. and Shen, H.G., "Modeling solar-driven ejector refrigeration system offering air conditioning for office buildings", Energy Build., Vol. 41, pp. 175–181, 2009.

[10] Sumeru, K., Sulaimon, S., Nasution, H. and Ani, F.N., "Numerical and experimental study of an ejector as an expansion device in split-type air conditioner for energy savings", Energy Build., Vol. 79, pp. 98–105, 2014.

[11] Śmierciew, K., Gagan, J., Butrymowicz, D. and Karwacki, J., "Experimental investigations of solar driven ejector air-conditioning system", Energy Build., Vol. 80, pp. 260–267, 2014.

[12] Ding, Z., Wang, L., Zhao, H., Zhang, H. and Wang, C., "Numerical study and design of a two-stage ejector for subzero refrigeration", Appl. Therm. Eng., Vol. 108, pp. 436–448, 2016.

[13] Zhang, K., Chen, X., Markides, C.N., Yang, Y. and Shen, S., "Evaluation of ejector performance for an organic Rankine cycle combined power and cooling system", Appl. Energy., Vol. 184, pp. 404–412, 2016.

[14] Liu, J., Wang, L. and Jia, L., "A predictive model for the performance of the ejector in refrigeration system", Energy Convers. Manag., Vol. 150, pp. 269–276, 2017.

[15] Hou, W., Wang, L., Yan, J., Li, X. and Wang, L., "Simulation on the performance of ejector in a parallel hybrid ejector-based refrigerator-freezer cooling cycle", Energy Convers. Manag., Vol. 143, pp. 440–447, 2017.

[16] Kitrattana, B., Aphornratana, S., Thongtip, T. and Ruangtrakoon, N., "Comparison of traditional and CRMC ejector performance used in a steam ejector refrigeration", Energy Procedia., Vol. 138, pp. 476–481, 2017.

[17] Liu, Y., Fu, H. and Yu, J., "Performance study of an enhanced ejector refrigeration cycle with flash tank economizer for low-grade heat utilization", Appl. Therm. Eng., Vol. 140, pp. 43–50, 2018.

[18] Kumar, V. and Sachdeva, G., "1-D model for finding geometry of a single phase ejector", Energy., Vol. 165, pp. 75–92, 2018.

[19] Mohammadi, A., "An investigation of geometrical factors of multi-stage steam ejectors for air suction", Energy., Vol. 186, 115808, 2019.

[20] Chen, G., Ierin, V., Volovyk, O. and Shestopalov, K., "Thermodynamic analysis of ejector cooling cycles with heat-driven feed pumping devices", Energy., Vol. 186, 115892, 2019.

[21] Nguyen, V.V., Varga, S., Soares, J., Dvorak, V. and Oliveira, A.C., "Applying a variable geometry ejector in a solar ejector refrigeration system", Int. J. Refrig., Vol. 113, pp. 187–195, 2020.

[22] Zhang, J., Zhai, X. and Li, S., "Numerical studies on the performance of ammonia ejectors used in ocean thermal energy conversion system", Renew. Energy., Vol. 161, pp. 766-776, 2020.

[23] Ruangtrakoon, N. and Thongtip, T., "An experimental investigation to determine the optimal heat source temperature for R141b ejector operation in refrigeration cycle", Appl. Therm. Eng., Vol. 170, 114841, 2020.

[24] Stark, J.P., "Fundamentals of classical thermodynamics", J. Chem. Educ., Vol. 43, A472, 1966.

[25] Daneshyar, M., "Solar radiation statistics for Iran", Sol. Energy., Vol. 21, pp. 345–349, 1978.

[26] Duffie, J.A. and Beckman, W.A., "Solar engineering of thermal processes John, Wiley", New York., 1991.

[27] Talebizadeh, P., Mehrabian, M.A. and Abdolzadeh, M., "Prediction of the optimum slope and surface azimuth angles using the Genetic Algorithm", Energy Build., Vol. 43, pp. 2998–3005, 2011.

[28] Mahmoodi, A.M. and Golnshan, A.A., "Investigation of Thermal Performance of Unglazed Transpired-Plate Solar Collectors in Perpendiclar Wind", NECjournals, Vol. 13, pp. 11-22, 2010.

[DOR: 20.1001.1.23452951.1400.11.4.2.1]

[DOI: 10.22052.11.4.60]